ACS OMEGA

http://pubs.acs.org/journal/acsodf

Article

Piezoelectric Effect and Ignition Characteristics of Coal Mine Gob Roof Collapse

Ya-nan Wang, De-ming Wang,* Hai-hui Xin,* Yun-fei Zhu, Zhenhai Hou, Wei Zhang, and Min Li

Cite This: *ACS Omega* 2021, 6, 28936−28945

Read Online

ACCESS | Metrics & More | Article Recommendations

ABSTRACT: Existing studies of coal self-ignition and impact frictional sparks do not provide valid support for the analysis of ignition sources in all cases of methane explosions in the gob. In this paper, the explosion in the gob of the Renlou coal mine is used to investigate the piezoelectric effect and ignition characteristics of roof collapse in identifying a new ignition source of gas explosion. Experimental and theoretical analyses conclude that the piezoelectric effect is produced by quartz, which is the main constituent of the roof sandstone. During the loading process, the piezoelectric effect and compressive strength are key factors in the gathering of free charges on rock tips. During rupture, the rock tip retains a large number of charges, forming a ″point-surface″ effect, which triggers an electron avalanche accompanied by an orange-yellow spark lasting over 22 ms, far exceeding the ionization energy and ignition induction period of methane−air mixtures. The piezoelectric effect and compressive strength of the rock cause the generation of electrical sparks, which is the ignition source of the explosion in the gob of Renlou mine II7$_3$22.

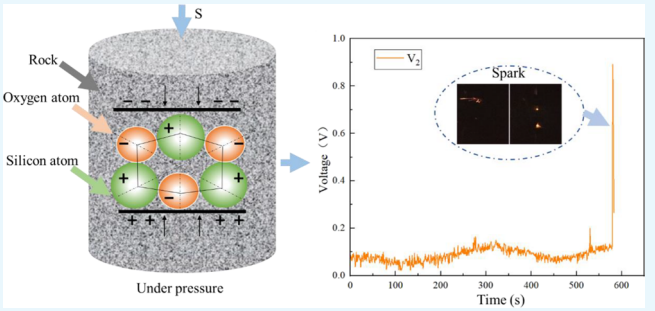

1. INTRODUCTION

Coal is the major energy source in many countries.[1] In recent years, although the safety situation of coal mines around the world has improved significantly, serious accidents in coal mines occur occasionally, and the coal mine safety situation remains serious.[2,3] As far as China is concerned, from 2010 to 2021, 55 serious coal mine thermodynamic accidents have occurred, with 1074 fatalities, including 27 accidents (49.09%) in the gob and working face, with 508 fatalities (47.3%). Due to the geological complexity of underground mining, the prevention of gas explosions in gob has always been the focus and difficulty of coal mine safety. It is necessary to further investigate the ignition sources in gobs to achieve better prevention of gas explosions in the coal mining industry.

Gob is a specific space formed by the collapse and accumulation of rock on the top of a coal seam after mining. The extent of filling depends on a number of factors including the height of the rock fall down (seam thickness or mining height), type of roof rock, and properties of rock strength as well as the distance from the front coal working face and depth of mining exploitation carried out.[4] As a result, there are empty voids (gaps between bent rock blocks) in the gob, and gas can flow inside. In addition, a small amount of coal will be left in the gob during the mining process. Therefore, the coexistence of coal and gas in the gob has prompted a great deal of research on coal spontaneous combustion leading to gas explosions.[5−8] Xu et al.[9] used large-scale coal low temperature self-ignition tests to measure parameters such as the oxygen consumption rate of coal and delineate the risk zone for coal self-ignition of relict coal in gobs. Zhou[10] studied the hazard area of coal and gas formation and analyzed the characteristics of the four-site intersection area of the coal mining crack field, CH_4 concentration field, O_2 concentration field, and ambient temperature field in the gob. Zhou[11] conducted a study on the self-ignition heating and explosion characteristics of a high-gas and easily spontaneous combustion coal seam and analyzed the effect of heat and mass transfer of multicomponent gases in the mining site on coal self-ignition. Many of the above studies have focused on gas explosions caused by coal self-ignition. However, it should be noted that the minimum temperature for the ignition of gas is 650 °C. If coal self-ignition is used as the ignition source, its temperature should reach 650 °C or more, at which time the coal is already burning. Prior to this need to undergo a fairly long heat storage process, there must be a continuous increase in the concentration of coal spontaneous combustion indicator gases (CO, C_2H_4, C_2H_2) and visible signs of ignition such as smoke and odor. If the

Received: July 26, 2021
Accepted: October 11, 2021
Published: October 21, 2021

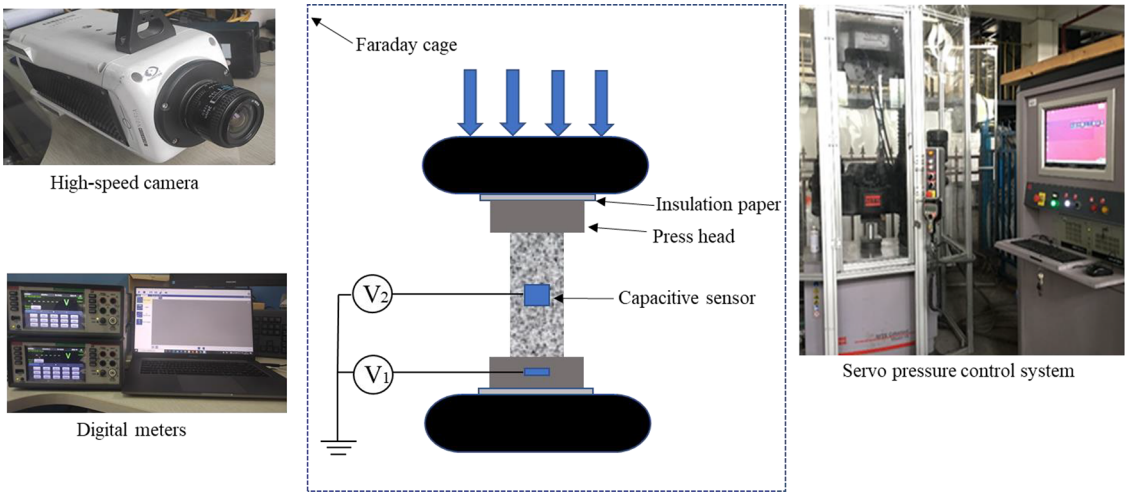

Figure 1. Schematic diagram of the rock sample discharge experiment system.

accident occurred without signs, the direct identification of coal self-ignition as the source of ignition would be unfounded.

Impact frictional sparks can also cause methane explosion in the gob. Ward et al.[12] used drop hammer experiments combined with infrared thermometry to show that frictional heat generation in rocks is closely related to the content of hard components such as quartz, rock chips, and feldspar. Xu et al.[13,14] studied the frictional temperature rise characteristics of rocks with different quartz compositions and internal structures and concluded that the value of the temperature rise at the frictional contact surface of rocks is proportional to the quartz content. Wang et al.[15] collected the instantaneous infrared radiation temperature of rocks during rock friction and impact by infrared thermography, established a mathematical model of the time−effect relationship between the rock surface temperature rise and temperature decay, and concluded that the methane explosions in gob is related to the rock surface temperature rise and spark. The relevant studies above all point to the high-speed friction and impact of the roof causing methane explosions mainly due to the thermal effect on the rock surface and the generation of molten sparks. However, the rock composition is mainly silica, whose melting point is above 1700 °C, and it is more difficult to form such conditions in the gob.

In summary, existing studies of coal self-ignition and impact frictional sparks do not constitute valid support for the analysis of ignition sources in all cases of methane explosion in gobs. Based on extensive investigations of gob explosions in coal mines such as UBB in the United States and Baijigou, Babao, and Renlou in China and review of relevant studies on electric sparks, the authors found that gob gas explosions occur in the above mines, the roofs are usually harder and thicker quartz sandstone, and the time of occurrence is usually during the periodic pressure. Its roof fracture and collision will generate electric sparks, with the possibility of igniting the methane.

The phenomenon of electrical sparks generated by the piezoelectric effect during the rock fracture and collision has been studied for a long time. Brady and Rowell[16] published an article in the journal Nature, recorded the phenomenon of electrical sparks from rocks in the laboratory, and hypothesized that rock fracture would affect the ignition of combustible gases. Kato et al.[17] studied the spatial properties of luminescence in rocks and suggested that the piezoelectric properties of quartz in rocks are the main reason for their luminescence during the plastic deformation phase. Takaki and Ikeya[18] suggested that the rock generates electrical sparks mainly due to stress changes releasing piezo-compensating bound charges, resulting in a strong electric field at the fracture zone. Widom et al.[19] suggested that mechanical energy is converted to electric field energy through piezoelectric effects during rock fracture and that the radiofrequency electric field accelerates condensed electrons, which collide with protons to produce neutrons and neutrinos and release large amounts of energy.

In conclusion, the electrodynamic effects of rocks have been studied in depth by previous authors. However, these studies have mainly focused on the luminescence of rocks in the air and have not involved the methane environment. The characteristics of electrical ignition caused by load fracture discharge during the mining of coal roof are poorly understood. Therefore, this paper tests the basic physical properties of rocks, constructing a complete set of rock discharge experimental systems from the piezoelectric ignition mechanism to investigate the piezoelectric effect of roof deformation and fracture igniting the methane characteristics, to provide new ideas for the prevention and control of gas explosions in the gob, which will be important for revealing the mechanism of gas explosions in the stope.

2. EXPERIMENTAL SECTION

2.1. Rock Sample. The rock samples were selected from the roof of the Renlou coal mine $II7_322$ gob in Anhui Province, China, and made into cylinders of $\varphi 50 \times 100$ mm, with an average sandstone density of 2.73 g/cm^3. The rock samples were placed in a drying cabinet at 80 °C for 12 h to remove moisture from the pores.

2.2. Mineral Composition and Surface Morphology. An X-ray diffractometer (XRD, D8 Advance, Bruker) was used to analyze the mineral composition of samples. Scanning electron microscopy (SEM, JSM-6390, JEOL) was used for comparative analysis of the surface morphology of the rock samples at different locations and magnifications.

2.3. Rock Discharge Experiment System. The experimental system is shown in Figure 1. A hydraulic universal testing machine (MTS-C64.605, Mattes Industry Co., Ltd.) was used for the uniaxial compression experiments with the

https://doi.org/10.1021/acsomega.1c03987
ACS Omega 2021, 6, 28936−28945

loading rates set at 0.5 and 5 kN/s. The rock sample was placed in the middle of the press head, and the ends of the press head in contact with the tester were insulated with insulating paper. To reduce external electromagnetic interference, we placed the rock samples in a grounded Faraday cage. A digital multimeter (DMM6500, Keithley) and a computer were used for signal acquisition. The lower end of the press was connected to one end of the digital multimeter to test the voltage generated during the loading of the rock sample, noted as V_1, and the other end was grounded. A capacitance sensor, made of a thin 30×30 mm copper sheet located 1 mm from the rock sample and connected to one end of a digital multimeter, was arranged parallel to the surface of the rock sample. It is used to capture the voltage change resulting from charges released of the rock surface during the loading, noted as V_2, and the other end is grounded. A high-speed camera (Phantom V211, Vision Research, USA) was used to record the electrical sparks generated by the destruction of the rock samples against a dark background. Three samples were tested at different loading rates to ensure the reliability of the experiments.

3. RESULTS AND DISCUSSION

3.1. Sandstone Composition and Surface Morphology. As can be seen from Figure 2, the quartz content of the

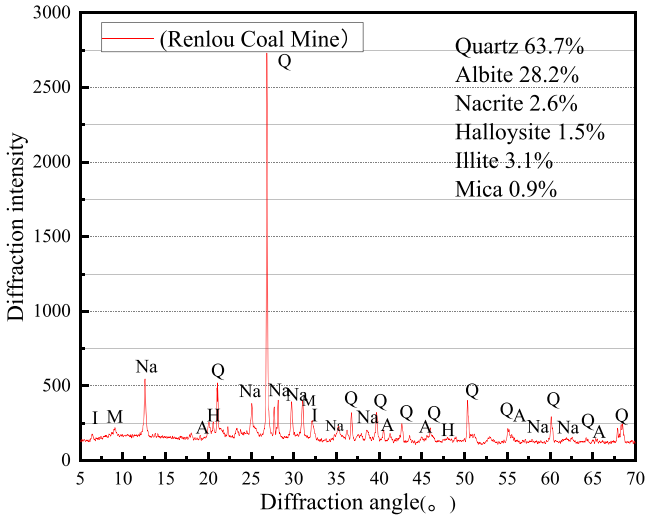

Figure 2. XRD results of roof sandstone in the Renlou coal mine.

Renlou mine sandstone is high, accounting for 63.7%, with feldspar (Na_2O-Al_2O_3-$6SiO_2$) content accounting for 28.2%, forming the basic skeletal structure of the sandstone. The Renlou mine sandstone also contains a small amount of mica, which is an aluminosilicate mineral with a continuous layered silicon-oxygen tetrahedral structure, the main component of which is also SiO_2. It belongs to siliceous cementation and has strong compressive resistance.

The SEM results of the rock sample at different magnifications are shown in Figure 3. There are many irregular, columnar, or granular shiny white areas on the surface of the sample, which is quartz. It has the characteristics of sedimentary rock, with fine grains and insignificant angles, and the grains are closely bound to the cementation, with high compressive strength. Due to the directional development of quartz, these rocks all have a strongly laminated lattice structure. At the microscopic and macroscopic scales, this strongly developed lamellar structure indicates that these rocks are strongly anisotropic and can produce piezoelectric effects. For the hard sandstone roof with a quartz component, the piezoelectric effect has a non-negligible effect on the generation of free charges.[20,21]

3.2. Piezoelectric Characteristics of Sandstone. Based on the above analysis of the basic physical properties of the sandstone at the Renlou mine, under the periodic pressure of the gob roof, the quartz crystals in the sandstone rapidly deform, generating bound charges proportional to the pressure, creating a great electrostatic field on the pressure surface of the rock. Bound charges will discharge when the roof collapses, triggering electronic avalanches and igniting the methane−air mixture. To verify the above ignition mechanism, uniaxial compression experiments were carried out on the sandstone to observe the voltage variation. Figure 4 shows the discharge patterns of Renlou mine sandstones at two loading rates of 0.5 and 5 kN/s. Table 1 shows the peak voltage, loading time, and peak pressure during the damage phase of the Renlou mine sandstone at different loading rates. Observing the variation of voltage V_1 at the two loading rates, it can be found that at a loading rate of 0.5 kN/s, there are four stages, depending on the curvature of the test result curve. In the first stage, as the stress increases, V_1 increases relatively rapidly, and the rock is in the compacting stage, with the original internal cracks gradually closed. As the stress increases, the voltage curve enters the second stage, when the rock is in the elastic deformation phase, and the voltage of the rock sample increases as the stress is applied. As the stress continues to increase, the voltage curve enters the third stage, when the rock is in the elastoplastic deformation stage, and it can also be observed that the voltage does not increase at this stage in a similar way to that in the second stage, and the voltage value remains approximately constant. Finally, the stress value continues to increase, and the voltage curve enters the fourth stage, when the rock is in the destruction phase, and the voltage rapidly reaches a peak and then decreases, and the peak duration is very short. At a loading rate of 5 kN/s, the first three stages of the voltage V_1 approximate a rising straight line due to the increase of the loading rate. Comparing the variation of V_2 at two loading rates of 0.5kN/s and 5kN/s, it can be seen that the voltage V_2 has a larger fluctuation and a higher frequency of change during the high-speed loading process, indicating that the rate of change of the electric field on the rock surface increases with the increase of the loading rate. At the moment of destruction of the rock sample, the rise in V_1 and V_2 values is surging and transient, which is typical of the electron avalanche phenomenon.

Throughout the compression process, if the whole rock is considered a whole, the polarization distribution of charges during the first three stages of compression and deformation of the rock can be simplified to a parallel plate capacitor, as shown in Figure 5. When the rock is deformed under pressure, an electric field is generated inside the rock due to the piezoelectric effect, which gradually increases with stress and produces a progressively stronger magnetic field, which causes the surrounding free charges to be stored and gathered in quartz-rich sites. As can be seen from the comparison of voltages in Figure 4a,b, the faster the rate of pressure applied, the faster the electric field changes, the greater the magnetic field generated, the greater the energy accumulated, and the greater the number of charges released at the moment of fracture.

https://doi.org/10.1021/acsomega.1c03987
ACS Omega 2021, 6, 28936−28945

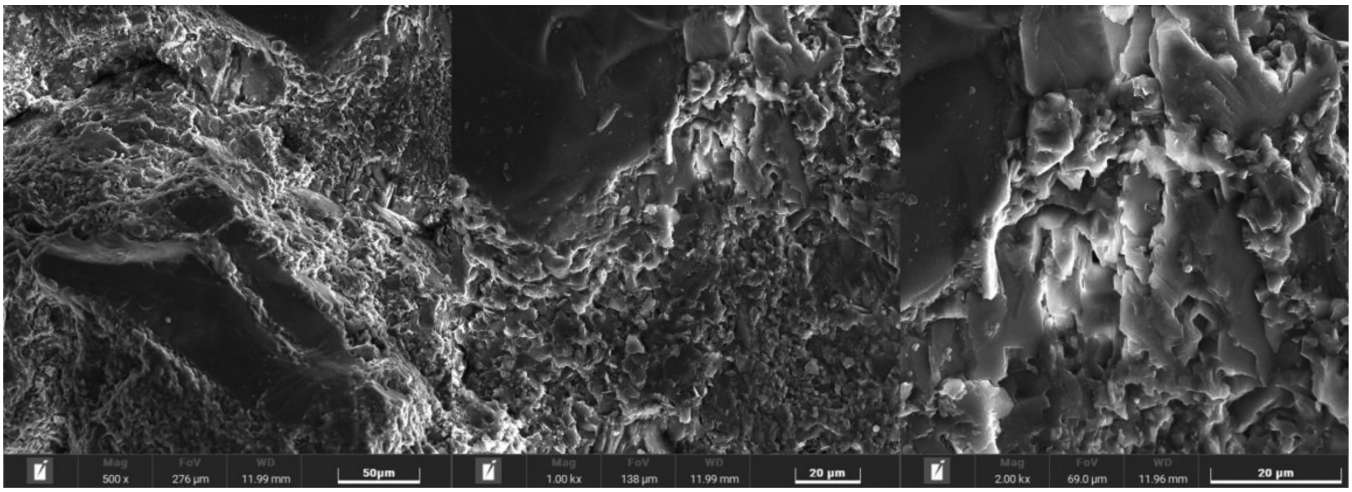

Figure 3. SEM images of the rock samples at different magnifications.

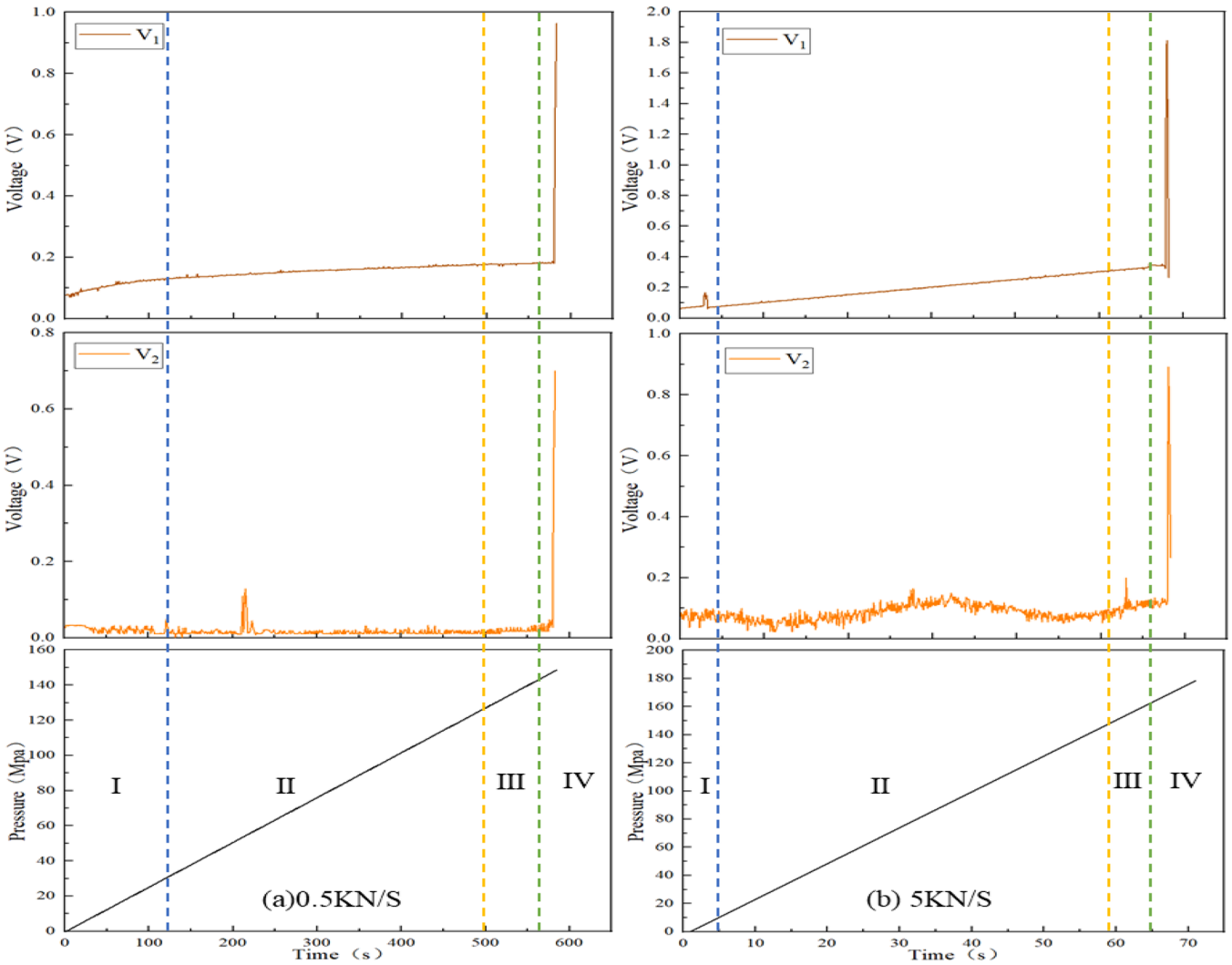

Figure 4. Discharge patterns of Renlou mine sandstones at two loading rates of 0.5 and 5 kN/s.

The eventual macrofracture damage of rock is closely related to the development and accumulation of microfractures. With increasing axial stress, the small ruptures within the sandstone specimen will become more and more violent. During the damage phase, the degree of internal microfracture will increase dramatically, expanding into each other to develop cracks, which lead to the formation of fracture surfaces. The rough surface formed on the fracture surface is conducive to inducing electrical discharges, and sparks are first to appear in areas of high curvature. This is due to the fact that the

https://doi.org/10.1021/acsomega.1c03987
ACS Omega 2021, 6, 28936−28945

Table 1. Peak Voltage, Loading Time, and Peak Pressure during the Damage Phase of the Renlou Mine Sandstone at Different Loading Rates

loading rates (kN/s)	specimen	V_{1max} (V)	V_{2max} (V)	T_{max} (s)	P_{max} (MPa)
0.5	1	1.1	0.52	582.5	148.4
	2	1.3	0.7	610.3	155.4
	3	1.21	0.59	570.2	145.2
5	1	1.78	0.826	70.3	178
	2	1.91	0.891	74.1	187.7
	3	1.83	0.89	75	189.9

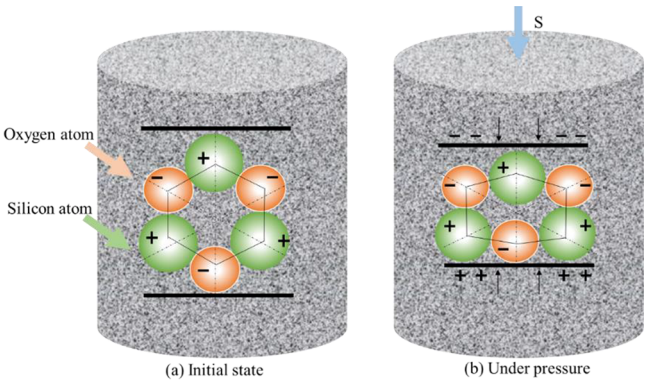

Figure 5. Polarization distribution of charges.

curvature has a higher charge surface density, and the electric field is stronger where the charge surface density is high. According to experiments and calculations by Freund et al., it is believed that up to a $10^{17}-10^{18}$ amount of electrons can be gathered at the rock tip.[22] When the tip of the broken rock is rich in quartz and has a large curvature close to one of the rock surfaces, a "point-surface" effect is created, resulting in a high voltage, breaking down the air and creating an electron avalanche.

3.3. Electric Spark Characteristics of Sandstone. The sandstone produces sparks along with the electron avalanche phenomenon, and the typical spurting sparks are shown in Figure 6. This figure first appeared in a thesis.[23] The authors found that the electric sparks appear in the form of jets and dots and generally occur in the rock disintegration phase. The light is emitted from the brittle fracture, and its location appears spatially distributed at 1−2 cm from the rock surface, with sparks of 1−3 cm in length, all of which are orange-yellow and last for more than 22 ms.

When rock disintegration and the electric field are strong enough in a local area, its air composition is no longer stable and ionization occurs, and electrons outside the nucleus become unbound from the nucleus by the electric field and flow in the direction of higher voltage, knocking out electrons from around stable orbiting gas molecules. Thus, under the combined effect of the electric field and free electron impact, many electrons move in the same direction to form a streamer. The air is broken down, the flying electrons may be caught by distant gas molecules, and the electrons fall from a high energy state to a low energy state. The annihilation of positive and negative electrons into photons is shown in Figure 7. All the

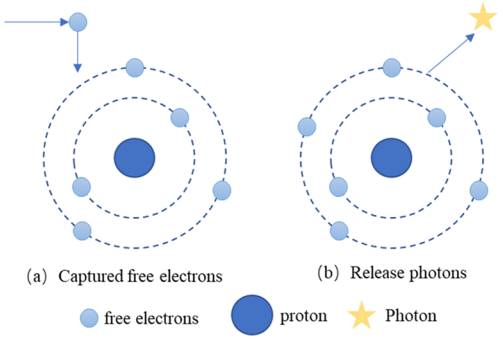

Figure 7. Photon emission process.

intrinsic energy (corresponding to the rest mass) is converted into photonic energy, i.e., electromagnetic radiation energy (the corresponding mass is the dynamic quality of the photon), which is the photoelectric effect and the cause of the electric spark.

There are two recognized theories of the mechanism of electrical spark ignition: the thermal theory of ignition, which treats the electrical spark as an applied high-temperature heat source, and the electrical theory of ignition, which suggests that the gas mixture ignition is caused by the ionization of the spark and the formation of an activation center, which provides the conditions for a chain reaction. As a result of the chain reaction, the gas mixture burns up.

For the above arguments, some scholars believe that the flash during the rock crushing process belongs to the discharge phenomenon of the gas medium. The ionization of different gases produces different colors of light, of which nitrogen is red and oxygen is yellow. The predominant color of the visible light is orange-yellow, as shown in Figure 6, indicating that the electric sparks had ionized nitrogen and oxygen, which is also consistent with Kato's conclusion that sparks were produced when the granite was compressed.[17,24] In addition, Brady and Rowell[16] measured the electron energy released in the rock fracture experiment to be greater than 23 eV. In comparison,

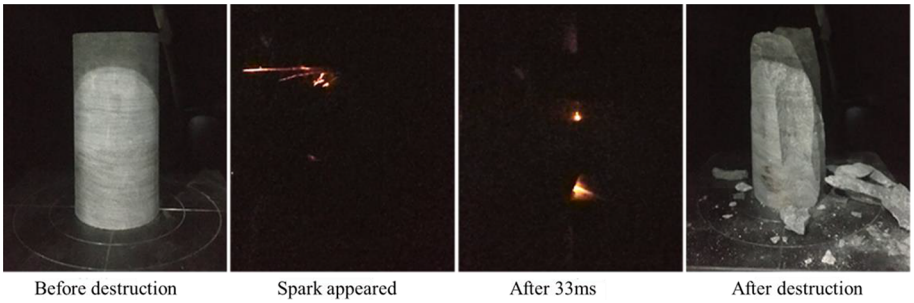

Figure 6. Spark produced by the roof sandstone.

https://doi.org/10.1021/acsomega.1c03987
ACS Omega 2021, 6, 28936−28945

the ionization energy of nitrogen is 15.6 eV and that of oxygen is 12.2 eV, so nitrogen and oxygen will be ionized. In contrast, the dissociation energies of the four C−H bonds of CH_4 are relatively low, not exceeding 4.6 eV, so the mixture of methane−air at the location of the spark must be ionized.

Some scholars have based on the brightness of the spark channel and the measurement of the spark energy, indicating that the temperature of the gas inside the spark channel can reach 10^4 °C,[25−27] which is sufficient to cause thermal ionization of the gas. The electrons on the periphery of oxygen, methane, and nitrogen molecules do not even need an electric field. They can be ionized from the nucleus by thermal motion itself. During the destruction phase of the rock, due to a large amount of light and electromagnetic waves emitted in a short time, the surrounding air is heated, and it expands rapidly. This expansion squeezes the surrounding air and quickly forms a high-pressure area, and the pressure in the spark channel can reach very high values, which in turn further promotes the ionization of the gas mixture.

In summary, the authors conclude that two mechanisms exist simultaneously in the process of ignition of gas by the piezoelectric effect of rock. Before the spark is formed, ionization is dominant, but when the spark is formed, there is a combination of ionization and thermal effects. Also, Lintin's experiments on the ignition characteristics of combustible gas mixtures indicate that for a methane−air mixture with a methane concentration of 9.4%, the shortest discharge duration that can maintain continuous propagation of the initial flame and develop into an ignition source is 2 ms at an instantaneous ignition energy of 0.5 mJ.[28] The time scales of the particle reactions are shown in Figure 8. The discharge in the gas mixture (CH_4, O_2) produces a large number of particles. Among these are ions such as CH_4^+, CH_3^+, CH_2^+, O_2^+, O^+, reactive radicals such as $H^\cdot$, $O^\cdot$, $OH^\cdot$, $^\cdot CH$, $^\cdot CH_2$, $^\cdot CH_3$, etc., and excited state molecules and atoms. There are intermediate components, such as alkanes and hydrogen, and intermediate oxides, such as CH_2O, CH_3OH, and CH_3O. There are final oxides, such as CO, CO_2, H_2O, etc.[29] Every particle is created and consumed. On the nanosecond time scale, electrons collide with molecules to ionize, dissociate, and excite them to generate a large number of active particles. On the microsecond and millisecond time scales, ion−molecule, reactive radical−molecule, and excited state molecule de-excitation reactions occur mainly, resulting in a reduction in the number of ions, reactive radicals, and excited state molecules. When the oxygen content is sufficient, i.e., within the explosive limit, ionization generates a large amount of O·, which reacts with various neutral molecules in a very rapid chemical process, allowing the free radicals to form a chain reaction. CH_4 was successfully ignited on a time scale of microseconds to milliseconds. The duration of the electric spark in the experiment was more than 22 ms, far longer than the induction period for the ignition of the methane−air mixture. Therefore, the spark is sufficient to ionize CH_4 to form a large number of free radicals and make the chain reaction self-sustaining in this time dimension, eventually causing the gas combustion explosion.

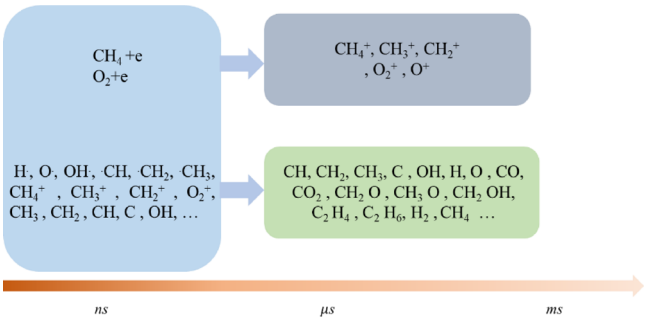

Figure 8. Time scale of particle reactions.

4. CASE STUDY

In 2014, a methane explosion accident occurred in the Renlou coal mine, killing three people. The methane explosion occurred without any warning. After the accident, the mine technicians took a series of measures to suppress the coal self-ignition of the gob, but four successive gas explosions continued to occur in the gob.

4.1. Mine Overview and Accident Process. The Renlou coal mine is a coal and gas outburst mine. The accident site is located in the II2 mining area, including coal seams 7_2, 7_3, and 8_2, which are self-ignition coal seams. The minimum spontaneous combustion ignition period for all coal seams is more than 6 months. The coal seam 7_2 was mined first as an upper protection layer, then coal seam 7_3, and finally coal seam 8_2. The II2 mining area is mined using a single wing uphill. The mining area track uphill, return wind uphill, and transportation uphill are all arranged in the bottom rock of

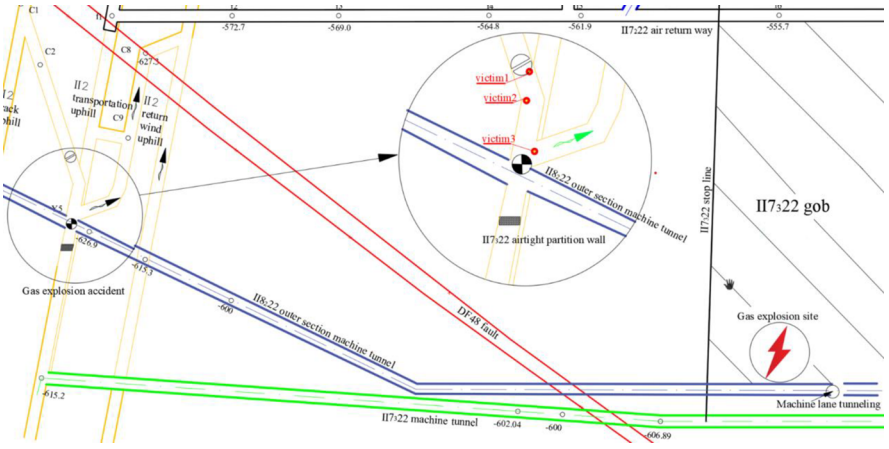

Figure 9. Gas explosion accident area.

https://doi.org/10.1021/acsomega.1c03987
ACS Omega 2021, 6, 28936−28945

the coal seam 8_2. There is a DF48 fault with a drop of 0−15 m approximately 50 m outward from the stop line of the II$7_2$22 and II$7_3$22 working faces.

The gas explosion accident area is shown in Figure 9. At 15:00 on 12 March 2014, 266 m of the outer section of the II$8_2$22 machine tunnel had been constructed, which exceeded the stop line of the II$7_3$22 working face and the stop line of the II$7_2$22 working face of 40 and 20 m, respectively. A gas explosion occurred within the II$7_3$22 gob. The shockwave damaged the airtight partition wall of the II$7_3$22 machine tunnel, killing three people who were transporting material for the outer section of the II$8_2$22 machine tunnel. Subsequently, there were several other gas explosions, but none of these caused any casualties. The exact explosion times are shown in Table 2.

Table 2. Exact Explosion Times of the II$7_3$22 Gob

explosion	date	time
1st explosion	12 March	15:09
2nd explosion	15 March	18:28
3rd explosion	15 March	20:18
4th explosion	15 March	22:09
5th explosion	17 March	17:11

4.2. Ignition Source Analysis. After the accident, no clear conclusion was given about the ignition source. Some experts believe that the self-ignition of the residual coal in the II$7_3$22 gob ignited the gas−air mixture. The authors have collected a large amount of data on the gob accident case and conducted on-site sampling and laboratory experiments. The analysis concluded that the real ignition source was the electrical sparks generated by the piezoelectric effect of the roof sandstone fracture under load. The further analysis is as follows.

4.2.1. Self-Ignition of the Residual Coal. The coal 7_3 and coal 7_2 are part of a proximity coal seam group with a spacing of 6.99 m. During the mining period of the II$7_3$22 working face, the roof rock layer is affected by mining and fault, fissures are developed, and more air leakage channels easily form in the II$7_3$22 gob. As a result, an explosive atmosphere is likely to form in the II$7_3$22 gob. However, during the 2 years and 6 months of mining in the II$7_3$22 coal seam, no coal self-ignition or gas explosion occurred in the gob. In order to inhibit the self-ignition of coal, the II$7_3$22 working face was poured with yellow slurry and sprayed with retardant 30 m away from the stop line, and after the coal seam was stopped, another 2340 m^3 of yellow slurry was poured into the II$7_3$22 gob. Therefore, it is very difficult to form coal self-ignition in the II$7_3$22 gob.

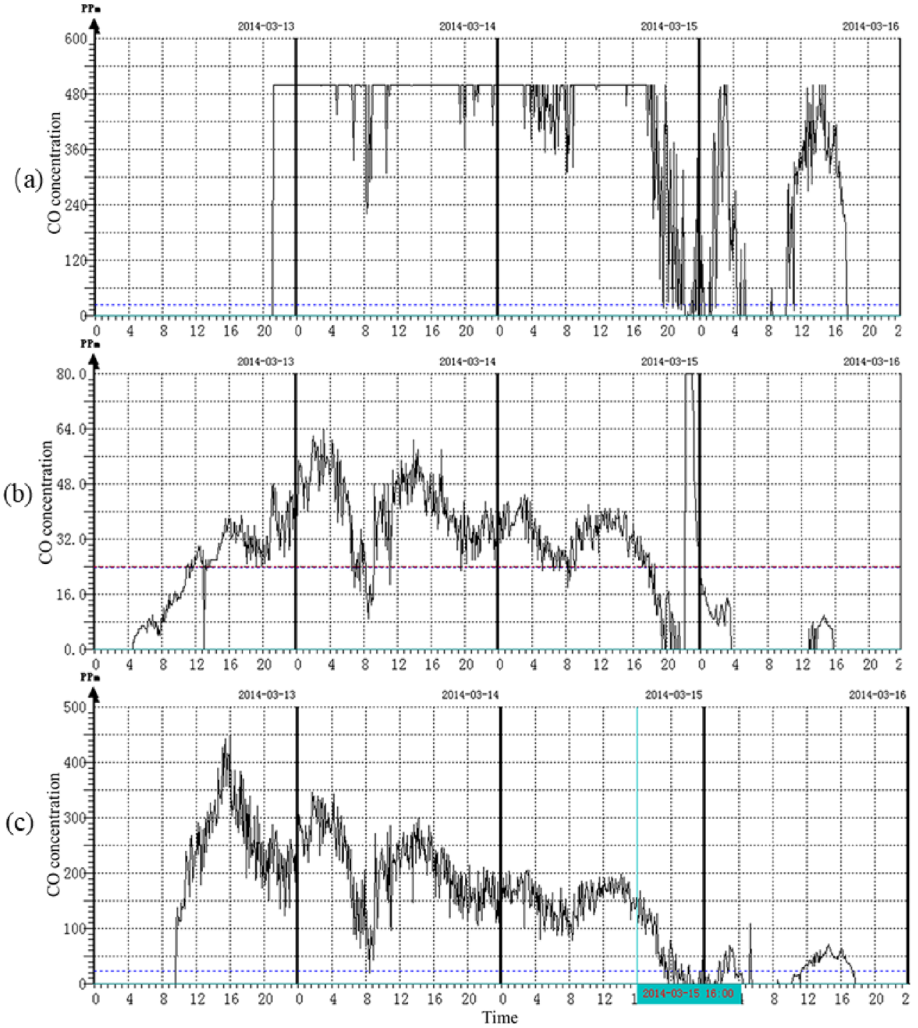

Figure 10. Variation trend of CO sensor data. (a) Airtight partition wall of the II$7_3$22 air return way; (b) main return airway of the II2 mining area.; (c) outer section of the II$8_2$22 air return way.

https://doi.org/10.1021/acsomega.1c03987
ACS Omega 2021, 6, 28936−28945

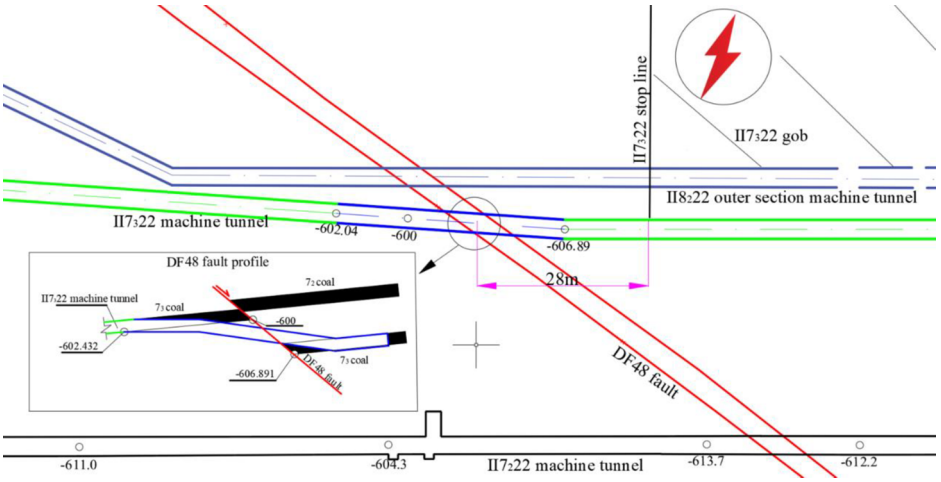

Figure 11. DF48 fault location map.

The trend of the data measured by the CO concentration sensor at the airtight partition wall of the II7$_3$22 air return way is shown in Figure10a. Prior to the accident, no abnormality was monitored by the CO concentration sensor. The first explosion was at 3 pm on 12 March. At this time, the CO concentration at the airtight partition wall of the II7$_3$22 air return way is zero. No CO was monitored until 9 pm on 13 March. During the subsequent explosion, the CO concentration remained high. Therefore, CO is not produced by the coal self-ignition. The high concentration of CO following the explosion indicates that the coal in the II7$_3$22 gob had been ignited as a result of the first explosion. Gas monitoring data from several other monitoring points can also be illustrated. Figure 10b shows the variation trend of CO sensor data in the main return airway of the II2 mining area. Figure 10c shows the variation trend of CO sensor data in the outer section of the II8$_2$22 air return way. This figure first appeared in a thesis.[23] These monitoring points all indicate that spontaneous combustion or combustion of the coal, if present, occurred after the gas explosion. Thus, the first and subsequent gas explosions were different in nature. The first was due to the presence of other ignition sources that ignited the gas, while the next four gas explosions were gas explosions caused by the compound combustion of gas−solid-phase combustibles.

When the accident occurred, the shock wave of the gas explosion was propagated along the II7$_3$22 machine tunnel and broke down the transport airtight partition wall. The shock wave killed three people who were transporting material for the outer section of the II8$_2$22 machine tunnel outside the airtight partition wall, while the airtight partition wall of the II7$_3$22 air return way was unaffected, as shown in Figure 9. This means that the source of the explosion is close to the gob near the stop line of the II7$_3$22 machine tunnel. From 12 February to 16 February, two water exploration and release holes were constructed at the working face to release approximately 500 m^3 of water from the II7$_3$22 gob. The 73 coal seam dips at 17°. Therefore, it can be determined that the coal was in a water saturated state close to the II7$_3$22 machine tunnel prior to the release of water. On 12 March, an explosion occurred in the mining area, only 25 days apart. The minimum natural combustion period of the II7$_3$22 coal seam is greater than 6 months. Therefore, the residual coal self-ignition in the gob near the stop line of the II7$_3$22 machine tunnel is basically impossible to occur.

4.2.2. Frictional Spark Ignites the Methane. Experimental studies have shown that the ignition of methane by frictional sparks from roof collapse requires continuous high-speed rotational friction between rocks, which is extremely demanding on the environmental conditions of the gob.[12−15,30,31] The explosion accident occurred in the II7$_3$22 gob. However, the II7$_3$22 coal seam is 2.3 m thick. It is mentioned in Section 1 that the high-speed friction and impact of the roof cause methane explosions mainly due to the friction thermal effect on the rock surface and the generation of molten sparks. The II7$_3$22 gob roof rock swing space is insufficient to create an environment for high-speed rock friction. Therefore, the possibility of ignition of the methane−air mixture by frictional sparks can be excluded.

4.2.3. Piezoelectric Effect Ignites the Methane. According to the on-site investigation data of the Renlou coal mine, the coal seams 7$_2$, 7$_3$, and 8$_2$ belong to the proximity coal seam. The II7$_2$22 machine tunnel, II7$_3$22 machine tunnel, and II8$_2$22 outer section machine tunnel all intersect the DF48 fault, as shown in Figure 11. The 7$_3$ coal has a drop of 6 m at the fault location. The DF48 fault is 28 m from the II7$_3$22 stop line. During the continuous tunneling of the outer section of II8$_2$22, the superimposed influence of the DF4 fault, the II7$_2$22 gob, and the mining pressure will cause great disturbance to the stress distribution of the rock layer behind the II7$_3$22 stop line. Combined with the comprehensive analysis of the electrical generation and discharge and spark characteristics of the coal mine roof sandstone in Section 3, it can be concluded that when the original stress equilibrium state of the roof sandstone was broken, the roof sandstone was extruded, deformed, and fractured under high pressure, and numerous fracture surfaces appeared instantly. These fracture surfaces retain a large number of charges due to the piezoelectric effect, forming a ″point-surface″ effect with the adjacent surface and generating a high voltage, which triggers an electron avalanche. The premixed gas−air mixture is large-scale breakdown, and electrical sparks are formed as shown in Figure 6. Thus, the methane−air mixture is ignited.

5. CONCLUSIONS

In this paper, based on the micro-mechanical analysis of sandstone samples from the Renlou mine, an experimental system was constructed, and an explosion accident analysis was conducted to investigate the possibility of a piezoelectric effect

https://doi.org/10.1021/acsomega.1c03987
ACS Omega 2021, 6, 28936−28945

igniting methane in the gob, with the following main conclusions:

(1) Before sandstone fracture, the piezoelectric effect and compressive strength are key factors in the gathering of free charges.
(2) At the moment of sandstone fracture, the rock tip retains a large number of charges, forming a "point-surface" effect, which triggers the electron avalanche.
(3) During the electron avalanche, the spark is orange-yellow and over 22 ms, far exceeding the ionization energy and ignition induction period of methane.
(4) The piezoelectric effect and compressive strength of the sandstone are the underlying causes, which determine the generation of electrical sparks and ignition of the gas explosion in the Renlou coal mine $II7_322$ gob.

AUTHOR INFORMATION

Corresponding Authors

De-ming Wang − *Faculty of Safety Engineering, China University of Mining & Technology, Xuzhou, Jiangsu 221116, China*; orcid.org/0000-0002-9954-6278; Email: dmwcumt@hotmail.com

Hai-hui Xin − *State Key Laboratory of Coal Resources and Safe Mining, China University of Mining and Technology, Xuzhou, Jiangsu 221116, PR China*; orcid.org/0000-0002-5315-0905; Email: xinxhh@cumt.edu.cn

Authors

Ya-nan Wang − *Faculty of Safety Engineering, China University of Mining & Technology, Xuzhou, Jiangsu 221116, China*

Yun-fei Zhu − *Department of Mining Engineering, Shanxi Institute of Technology, Yangquan 045000 Shanxi, China*

Zhenhai Hou − *Faculty of Safety Engineering, China University of Mining & Technology, Xuzhou, Jiangsu 221116, China*

Wei Zhang − *Faculty of Safety Engineering, China University of Mining & Technology, Xuzhou, Jiangsu 221116, China*

Min Li − *School of Resource, Environment and Safety Engineering, Hunan University of Science and Technology, Xiangtan 411201 Hunan, China*

Complete contact information is available at: https://pubs.acs.org/10.1021/acsomega.1c03987

Notes

The authors declare no competing financial interest.

ACKNOWLEDGMENTS

This work was supported by the National Natural Science Foundation of China (grant no. 51974299), the Key Program of the National Natural Science Foundation of China (grant no. 52130411), and the Independent Research Project of the State Key Laboratory of Coal Resources and Safe Mining, CUMT (SKLCRSM19X0013).

REFERENCES

(1) Brodny, J.; Tutak, M.; Michalak, M. A data warehouse as an indispensable tool to determine the effectiveness of the use of the longwall shearer. In *International Conference: Beyond Databases, Architectures and Structures*; Springer: 2017.
(2) Wang, D. Thermodynamic disasters and characteristics of coal mines. *J. China Coal Soc.* **2018**, *43*, 137−142.
(3) Wang, D. *Thermodynamic disasters in coal mines*. Science Press: 2018, p. 14−37.
(4) Tutak, M.; Brodny, J. Determination of particular endogenous fires hazard zones in goaf with caving of longwall. In *IOP Conference Series: Earth and Environmental Science*; IOP Publishing: 2017; *95*.
(5) Ma, D.; Qin, B.; Li, L.; Gao, A.; Gao, Y. Study on the methane explosion regions induced by spontaneous combustion of coal in longwall gobs using a scaled-down experiment set-up. *Fuel* **2019**, *254*, 115547.
(6) Li, L.; Qin, B.; Liu, J.; Leong, Y. K. Integrated experimentation and modeling of the formation processes underlying coal combustion-triggered methane explosions in a mined-out area. *Energy* **2020**, *203*, 117855.
(7) Chen, X.; Feng, S.; Wang, L.; Jia, Q. Distribution and prevention of CO in a goaf of a working face with Y type ventilation. *ACS Omega* **2021**, *6*, 1787−1796.
(8) Pan, R. K.; Li, C.; Yu, M. G.; Xiao, Z. J.; Fu, D. Evolution patterns of coal micro-structure in environments with different temperatures and oxygen conditions. *Fuel* **2020**, *261*, 116425.
(9) Xu, J. C.; Wen, H.; Zhang, X. H. Study on the method for determining dangerous zones of coal self-ignition in gobs in a fully mechanized top-coal caving face. *J. Univ. Sci. Technol. China* **2002**, *32*, 672−677.
(10) Zhou, F. B. Study on the coexistence of gas and coal spontaneous combustion(I): disaster mechanism. *J. China Coal Soc.* **2012**, *37*, 843−849.
(11) Zhou, X. Study on spontaneous combustion and explosion characteristics and prevention and control technology with high-gas and easily-spontaneous combustion coal seam in stope. *Liaoning Techno. Univ.* **2006**.
(12) Ward, C. R.; Crouch, A.; Cohen, D. R. Identification of potential for methane ignition by rock friction in Australian coal mines. *Int. J. Coal Geol.* **2001**, *45*, 91−103.
(13) Qu, Q. D.; Xu, J. L.; Ma, W. D.; Zhang, S. H.; Jiang, K. Experimental study on gas explosion detonated by the rock friction sparks. *J. China Coal Soc.* **2006**, *31*, 466−469.
(14) Xu, J.; Zhang, R.; Yu, B. Study on gas explosion induced by impact-friction sparks during roof collapse with fully-mechanized top-coal caving mining. *Int. J. Min. Sci. Technol.* **2007**, *36*, 12−16.
(15) Wang, J.-c.; Wang, J.-x.; Shen, J. Experimental research on gas hazard incident caused by roof collapse. *J. Min. Saf. Eng.* **2007**, 12−16.
(16) Brady, B. T.; Rowell, G. A. Laboratory investigation of the electrodynamics of rock fracture. *Nature* **1986**, *321*, 488−492.
(17) Kato, M.; Mitsui, Y.; Yanagidani, T. Photographic evidence of luminescence during faulting in granite. *Earth, Planets Space* **2010**, *62*, 489−493.
(18) Takaki, S.; Ikeya, M. A dark discharge model of earthquake lightning. *Jpn. J. Appl. Phys.* **1998**, *37*, 5016.
(19) Widom, A.; Swain, J.; Srivastava, Y. N. Neutron production from the fracture of piezoelectric rocks. *J. Phys. G: Nucl. Part. Phys.* **2013**, *40*, No. 015006.
(20) Aufort, J.; Aktas, O.; Carpenter, M. A.; Salje, E. K. H. Effect of pores and grain size on the elastic and piezoelectric properties of quartz-based materials. *Am. Mineral.* **2015**, *100*, 1165−1171.
(21) Casals, B.; Nataf, G. F.; Salje, E. K. H. Avalanche criticality during ferroelectric/ferroelastic switching. *Nat. Commun.* **2021**, *12*, 345.
(22) Freund, F. T.; Kulahci, I. G.; Cyr, G.; Ling, J.; Winnick, M.; Tregloan-Reed, J.; Freund, M. M. Air ionization at rock surfaces and pre-earthquake signals. *J. Atmos. Sol.-Terr. Phys.* **2009**, *71*, 1824−1834.
(23) Li, M. Study on the mechanical-electrical signature and ignition properties of coal mine goaf roof. *China Univ. Min. Techno.* **2020**.
(24) Yasui, Y. A study on the luminous phenomena accompanied with earthquake (part II). *Mem. Kakioka Mag. Obs.* **1971**, *14*, 67−77.
(25) Haberland, H. A model for the processes happening in a rare-gas cluster after ionization. *Surf. Sci.* **1985**, *156*, 305−312.
(26) Raizer, Y. P.; Braun, C. Gas Discharge Physics. *Appl. Opt.* **1991**, *31*, 2400−2401.

(27) Martelli, G.; Smith, P. N.; Woodward, A. J. Light, radio-frequency emission and ionization effects associated with rock fracture. *Geophys. J. Int.* **1989**, *98*, 397−401.
(28) Lintin, D. R.; Wooding, E. R. Investigation of the ignition of a gas by an electric spark. *Br. J. Appl. Phys.* **1959**, *10*, 159−166.
(29) Wang, H.; Gu, S.; Chen, T. Experimental investigation of the impact of CO, C_2H_6, and H_2 on the explosion characteristics of CH_4. *ACS Omega* **2020**, *5*, 24684−24692.
(30) Liang, Y.; Dai, J.; Zou, Q.; Li, L.; Luo, Y. Ignition mechanism of gas in goaf induced by the caving and friction of sandstone roof containing pyrite. *Process Saf. Environ. Prot.* **2019**, *124*, 84−96.
(31) Yao, L.; Ma, S.; Chen, J.; Shimamoto, T.; He, H. Flash heating and local fluid pressurization lead to rapid weakening in water-saturated fault gouges. *J. Geophys. Res.: Solid Earth* **2018**, 9084−9100.

https://doi.org/10.1021/acsomega.1c03987
ACS Omega 2021, 6, 28936−28945